Study on Seismic Performance of Integrated Support of Steel Arch and Anchor in Loose Surrounding Rock of Highway Tunnel

Zhigang Zhang[1], Xiyuan Liu[2(✉)], Chong Zhang[2], Jing Zhang[2], and Dongqiang Xu[2]

[1] Hebei Provincial Expressway Yan Chong Construction Office, Zhangjiakou, China
[2] School of Civil Engineering and Transport, Hebei University of Technology, Tianjin, China
liuxiyuan@hebut.edu.cn

Abstract. In order to study the seismic performance of the new support structure with the integration of steel arch and anchor rod under the bulk surrounding rock of highway tunnel, this paper takes Xinglinpu tunnel of Yanchong expressway as the engineering background and conducts the dynamic time-history analysis of the deformation, stress and plastic zone distribution of the tunnel second lining structure under the original support and the new support according to the specification and with the help of FLAC3D finite difference software. It is concluded that the seismic performance of the original support and the new support structure is basically the same. The new support structure reduces the number of anchors, the disturbance to the surrounding rock and the cost, so the new support structure is worth promoting.

Keywords: Highway tunnel · Scattered surrounding rock · Seismic performance · Dynamic response · Numerical simulation

1 Introduction

After the 21st century, the average annual growth rate of road tunnels in China was 20% [1]. With the increase in tunnel mileage, the number of tunnels built in mountain ranges in high-intensity seismic zones had reached a significant percentage. In 2008, 33 of the 56 tunnels near the earthquake area of the Wenchuan earthquake (magnitude 8.0) were damaged. The tunnel structure in the fault fracture zone and lining defect section was the most damaged, and it was difficult to repair after tunnel failure [2]. Therefore, it is necessary to carry out a systematic study of the seismic performance of road tunnels.

Qiangqiang Sun [3] carried out a dynamic non-linear time course numerical simulation of tunnel construction to investigate the effect of the construction-induced initial stress state on the seismic response of the tunnel. Longqi Yan [4] applied a two-dimensional transient dynamic finite element simulation technique to investigate the seismic response of a soil-structure interaction system under the oblique incidence of P- and SV-waves. Wang Mingnian [5] and Cui Guangyao [6] pointed out that the seismic damping of underground structures in high-intensity seismic zones can be done by

G. Feng (Ed.): ICCE 2021, LNCE 213, pp. 380–393, 2022.
https://doi.org/10.1007/978-981-19-1260-3_35

changing their structural properties or by installing a damping layer. By conducting a large shaking table model test study on the cavern section of the Galongla tunnel, Jiang Shuping [7] concluded that attention should be paid to the prevention and control of surrounding rock instability during the earthquake process to reduce the damage produced by the surrounding rock to the tunnel. Wang Qjuyi [8] proposed a comprehensive seismic measure of adding a damping layer between the initial support and the second lining and appropriately increasing the reinforcement of the second lining. Liang Bo [9] analyzed the dynamic response of road tunnel lining in mega-section and pointed out that the second lining could play a major role as a safety reserve during earthquakes. By analyzing different grouting schemes for highway tunnels, Based on the concrete plastic damage model, He Zegan [10] established a three-dimensional nonlinear finite element model of the tunnel-surrounding rock system and pointed out that the arch shoulder and arch waist of the lining structure are the weak parts of its seismic resistance. By performing dynamic time-history analysis of road tunnels, Liu Liyu [11] concluded that the acceleration response of the tunnel structure decreases when located on soft ground and poor surrounding rock, but larger stresses are generated.

The seismic performance of tunnels based on the new practical patent technology "Integrated support structure of steel arch and prestressed anchor rod for highway tunnel" invented by Xu Dongqiang [12] has not been studied in the above-mentioned existing tunnel seismic studies. This new support structure optimizes the arrangement of anchor rods (pipes), so that the steel arch, anchor rods (pipes), shotcrete and surrounding rock form an integrated structure, thus greatly improving the stability of the surrounding rock and support structure.

Therefore, this paper presents a dynamic time-history analysis of the deformation, stress and plastic zone distribution of the tunnel second lining structure under the original support and the new support.

2 Project Overview

The Xinglinpu tunnel is a highway separated long tunnel, located in the north of Xinglinbao, Huailai County, Zhangjiakou, which is one of the more difficult tunnels to construct with poor surrounding rock conditions in Yanchong expressway. The left and right sides of the Hebei section of the tunnel are both 1520 m. The average proportion of grade V surrounding rock is 44.5%, and the average proportion of grade IV surrounding rock is 43.8%. The broken bulk surrounding rock occupies 90% of the total length of the tunnel. The maximum burial depth of the tunnel is 480 m. The area to which the Xinglinpu tunnel belongs is a temperate subarid zone in the continental monsoon climate. The groundwater is localized by bedrock fracture water and dominated by pore diving. It is located in the middle mountainous area of igneous rocks. The stratigraphic rocks are mainly andesite and coarse andesite with developed joints and fissures, and quartz sandstone is locally present.

According to the *Seismic ground motion parameters zonation map of China* (GB18306–2015) [13] issued by the National Seismological Bureau, the area is a Class II site, with a 50-year exceedance probability of 10%, a seismic intensity of 8 degrees, a design basic ground vibration peak acceleration of 0.20 g and a characteristic period of 0.40 s for the ground vibration response spectrum.

3 Simulation Support Scheme

The original support structure scheme (hereinafter referred to as the original scheme) under grade V surrounding rocks is 28 hollow grouting system anchors per bay of steel arch, 2 hollow grouting 1ocking foot anchors on each 1eft and right arch waist, and grouting small conduits within 120° of the arch roof, with a grouting reinforcement radius of 1 m, as shown in Fig. 1(a).

The new support structure scheme for the tunnel under grade V surrounding rock is 2 rows of hollow grouting locking foot anchors per steel arch at the left and right arch shoulders of the tunnel, 1 row of hollow grouting foot locking anchors at the left and right arch waist and arch foot, two of them in each row. The grouting small conduit is laid at 120° at the top of the arch, and the radius of grouting reinforcement is 1m. Due to the poor condition of the surrounding rock, reinforced support is required at the top of the arch crown, so two different reinforced support schemes are used. As shown in Fig. 1(b), the new support structure scheme 1 (hereinafter referred to as new scheme 1) has 8 additional anchors of the hollow grouting system within 60° of the arch crown. As shown in Fig. 1(c), the new support structure scheme 2 (hereinafter referred to as new scheme 2) has 14 additional anchors of the hollow grouting system within 120 of the arch crown.

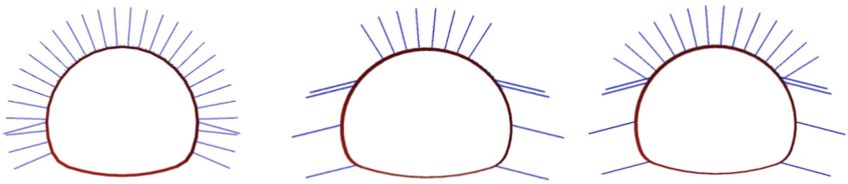

(a) The original (b) New scheme 1 (c) New scheme 2

Fig. 1. Support structure scheme

4 Establishment of Tunnel Model and Selection of Parameters

4.1 Establishment of Calculation Model

The simulations were carried out using FLAC3D for the dynamic time-history analysis of the tunnel. The model boundary is 50 m from the center point of the tunnel section to the bottom and left and right boundaries respectively, and the distance to the top

surface is taken to the surface, with a tunnel depth of 200 m. The inner contour of the tunnel calculation model section adopts the form of three center circles. The vertical effective height of the tunnel structure is 9.85 m, and the structural width is 12.1 m. As the longitudinal structure of the tunnel is continuous and regular, the cross-sectional configuration remains unchanged and the tunnel longitudinal direction is taken to be 6 m. Only the seismic checking calculation in the cross-sectional direction of the tunnel was performed.

After the tunnel excavation, initial support and second lining have been completed, seismic waves were applied to the tunnel structure as a whole to assess the seismic performance of the tunnel support structure by analyzing the deformation, stress and plastic zone distribution of the tunnel second lining structure.

4.2 Unit Type and Parameter Setting

Taking into account the preliminary geological survey report, construction conditions, advanced geological forecasts and the graded determination parameters of the surrounding rocks on site, and referring to the physical and mechanical parameters of the surrounding rocks at all levels specified in the specification [14], the specific parameters selected are shown in Table 1. In the actual project, the test section of the tunnel has about 24 m thick gravel soil layer at the surface, and below the gravel soil layer are all grade V surrounding rocks.

According to the relevant literature [15], the elastic modulus of the surrounding rock in the anchor grouting area increases by 50%, the Poisson's ratio decreases by 9%, the cohesion increases by 65% and the angle of internal friction increases by 3%. The modulus of elasticity of the surrounding rock in the small conduit reinforcement circle of grade V surrounding rock is increased by 2.6 times, Poisson's ratio is unchanged, internal friction angle is increased by 1.2 times, cohesion is increased by 2 times and density is increased by 10%. The surrounding rock is simulated in solid units, using an elastoplastic principal structure model and satisfying the Mohr-Coulomb yielding criterion.

Table 1. Enclosure rock and structural parameters

Material	Modulus of elasticity (GPa)	Poisson's ratio	Cohesive force (MPa)	Angle of internal friction (°)
Gravelly soil	0.80	0.48	0.15	18
Surrounding rock	1.15	0.37	0.19	26
Anchor grouting area	1.73	0.34	0.31	27
Small conduit reinforced ring surround	3.00	0.37	0.38	31
Initial lining	28.6	0.20	–	–
Second lining	33.5	0.20	7.20	60

The initial support for all three support schemes consists of reinforcement mesh, I18 I-beam steel arches (75 cm longitudinal spacing) and 24 cm thick C25 shotcrete. The second lining is C35 molded reinforced concrete with a thickness of 45 cm. Both system anchors and locking foot anchors are hollow grouted anchors.

The initial support for all three support schemes was simulated using shell cells. The second lining was simulated using solid units. Overrunning small conduits within 120° of the arch crown were simulated with beam units. The anchors were simulated using cable units. The modulus of elasticity was calculated by equating the steel arch, reinforcement mesh and C25 shotcrete layer in the primary lining as a single support as shown in Eq. (1):

$$E = \frac{s_c \cdot E_c + s_g \cdot E_g}{s_c + s_g} \tag{1}$$

Where E is the converted modulus of elasticity of concrete (GPa). E_c is the modulus of elasticity of the original concrete (GPa). E_g is the modulus of elasticity of the steel (GPa). s_g is the cross-sectional area of the steel (m^2). s_c is the concrete cross-sectional area (m^2).

The code [16] states that the dynamic modulus of elasticity of a tunnel structure is 30% higher than the static modulus of elasticity, so the modulus of elasticity in Table 1 will be increased by 30% for the dynamic calculations.

4.3 Setting of Boundary Conditions and Mechanical Damping

The surrounding rock at the bottom of the tunnel is a rigid foundation with the bottom of the model horizontal and all sides straight. The dynamic boundary conditions are selected as free-field boundaries, which are imposed via the Apply ff command stream.

The form of damping chosen for this simulation is local damping, with a local damping factor of 0.05. The local damping calculations can reach convergence values as quickly as possible, the calculation time is reduced and better results can be obtained without having to determine the frequency.

4.4 Selection of Seismic Waves

In this paper, El-Centro wave, Chinese Taiwan Chi-Chi (ChiChi) wave and Japanese Hanshin wave were selected for computational analysis. The most significant parts of peak acceleration and amplitude frequency were in the selected periods.

The seismic importance factor of road tunnels was selected concerning domestic and international standards for shield, open cut and immersed tunnels. Therefore, the seismic importance factor is taken as 1.0 when the design ground shaking is a 50-year exceedance probability of 10% and the recurrence period is 475 years. In this paper, the design basic ground vibration peak acceleration of the tunnel is 0.20 g. The seismic category of the highway tunnel is B. Therefore, for E1 earthquake, the seismic importance factor is 0.43, the recurrence period is 75 years, and the peak acceleration is 0.086 g. For E2 earthquake, the seismic importance factor is 1.3, the recurrence period is 1000 years,

and the peak acceleration is 0.26 g. The seismic wave adjustment equation is shown in Eq. (2):

$$a'(t) = \frac{a'_{\max}}{a_{\max}} a(t) \tag{2}$$

Where $a'(t)$ is the adjusted seismic acceleration time course of El-Centro wave. $a'_{\max}$ is the adjusted peak seismic acceleration of El-Centro wave. $\alpha(t)$ is the seismic acceleration time intervals recorded by El-Centro wave. α_{max} is the peak seismic acceleration recorded by El-Centro wave.

The seismic wave acceleration time course is adjusted and baseline corrected according to Eq. (2). The adjusted input seismic waves are shown in Fig. 2.

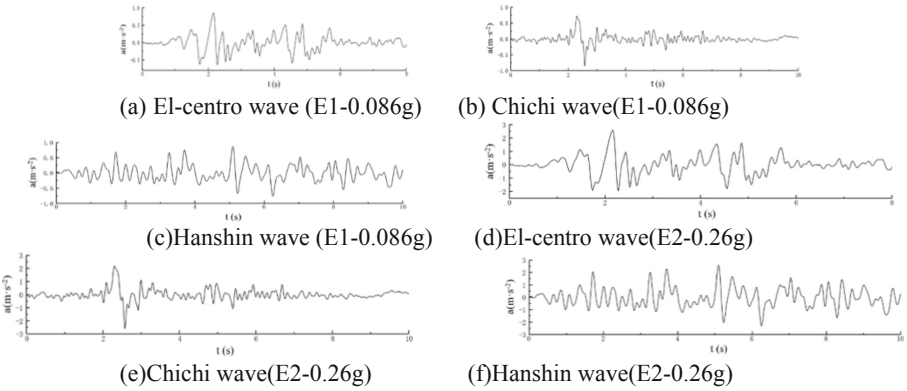

(a) El-centro wave (E1-0.086g) (b) Chichi wave(E1-0.086g)

(c)Hanshin wave (E1-0.086g) (d)El-centro wave(E2-0.26g)

(e)Chichi wave(E2-0.26g) (f)Hanshin wave(E2-0.26g)

Fig. 2. Acceleration time curve at E1 seismic action (0.086 g) and E2 seismic action (0.26 g)

5 Analysis of Numerical Simulation Results

The code proposes a "multi-level defense, two-stage design". The tunnel structure should meet performance requirement 1 under E1 seismic action, i.e. be in an elastic state and structurally intact before and after the earthquake. The tunnel structure should meet performance requirement 2 under E2 seismic action, that is, in an elastic to elastoplastic transition state, the structure can be slightly damaged locally, after reinforcement treatment to ensure the safety of the tunnel.

Strength testing of the tunnel structure for E1 seismic action is required to meet performance requirement 1. The tunnel structure is subjected to deformation and strength tests for E2 seismic action and its seismic performance meets the performance requirement 2.

5.1 Deformation Analysis of the Tunnel Second Lining Structure

The maximum convergence values of the tunnel second lining structure for the three support schemes for E2 seismic action are shown in Table 2.

Table 2. Maximum convergence values for each part of the tunnel under E2 seismic action (mm)

Seismic wave	Support scheme	Convergence of the arch shoulder	Convergence of the arch waist	Convergence of the arch foot
EL wave	The original	18.795	8.995	2.097
EL wave	New scheme 1	19.722	9.612	2.024
EL wave	New scheme 2	19.749	9.606	2.023
Hanshin wave	The original	39.917	19.603	4.542
Hanshin wave	New scheme 1	42.401	20.994	4.312
Hanshin wave	New scheme 2	42.279	20.980	4.306
CC wave	The original	21.408	9.584	2.155
CC wave	New scheme 1	22.666	10.403	2.076
CC wave	New scheme 2	22.650	10.412	2.071

The specification requires that the maximum convergence value of the second lining structure in a drill and blast tunnel during E2 seismic action is 5‰ of the tunnel span. In this project, the tunnel span is 12.10 m and the maximum convergence value is calculated to be 60.5 mm.

As can be seen from Table 2, the maximum convergence values of the second lining structure for the original, new scheme 1, and new scheme 2 are 3.30‰, 3.50‰, and 3.49‰ of the span respectively for the E2 seismic action. The difference between the maximum horizontal convergence values of the three schemes is small and the difference in deformation is not significant. The maximum convergence values for each support scheme are less than 60.5 mm for the shoulder, waist, and foot of the arch, and the tunnel structure is in a safe condition. Therefore, the convergence deformation of the tunnel second lining structure for all three support schemes in grade V rock meets the code's requirements.

5.2 Stress Analysis of Tunnel Second Lining Structure

Under E1 and E2 seismic action, the minimum peak principal stresses at each monitoring point of the tunnel second lining structure for the three support schemes are shown in Tables 3 and 4, and the maximum peak principal stresses are shown in Tables 5 and 6.

As indicated in Tables 3 and 4, the minimum peak principal stresses at each monitoring point of the second lining structure in the three support schemes are compressive, and they are all less than the standard value of dynamic compressive strength of C35 concrete of 28.08 MPa. Therefore, under E1 and E2 seismic action, the tunnel second lining structure did not produce compression damage.

As indicated in Tables 5 and 6, under E1 and E2 seismic action, the maximum value in the maximum principal stress peak at each monitoring point of the tunnel second lining structure is tensile stress, and all of them are less than the standard value dynamic tensile strength of C35 concrete of 2.64 MPa. Under E2 seismic action, the maximum peak principal stress at the arch shoulder and foot of the tunnel second lining structure is larger compared to other parts.

Since the tunnel structure is in a state of elastic to elastoplastic transition under E2 seismic action, the second lining principal structure model is the Mohr-Coulomb principal structure ideal elastic-plastic model. However, under the ideal elastic-plastic model, the maximum tensile stress value will not exceed the standard value of dynamic tensile strength of C35 concrete of 2.64 MPa. Therefore, whether the second lining structure is damaged in tension cannot be discerned only by whether the peak tensile stress exceeds 2.64 MPa. At this point, the distribution of the post-earthquake plastic zone of the second lining structure should be further analyzed to determine the part of the second lining structure that has been damaged.

Table 3. Peak value of minimum principal stress at monitoring point under E1 earthquake (MPa)

Seismic wave	Support scheme	Arch crown	Right arch shoulder	Right arch waist	Right arch foot	Arch base	Left arch foot	Left arch waist	Left arch shoulder
EL wave	The original	−2.059	−3.636	−5.749	−6.684	−0.093	−6.273	−5.880	−3.502
EL wave	New scheme 1	−2.097	−3.810	−6.744	−6.789	−0.100	−6.349	−6.557	−3.765
EL wave	New scheme 2	−2.103	−3.788	−6.788	−6.830	−0.086	−6.401	−6.703	−3.712
Hanshin wave	The original	−2.492	−6.276	−5.753	−9.291	−0.884	−8.905	−5.896	−6.073
Hanshin wave	New scheme 1	−2.503	−6.317	−6.798	−9.394	−0.747	−9.091	−6.671	−6.224
Hanshin wave	New scheme 2	−2.503	−6.271	−6.851	−9.451	−0.759	−9.138	−6.832	−6.145
CC wave	The original	−2.045	−3.541	−5.721	−6.818	−0.094	−6.218	−5.887	−3.806
CC wave	New scheme 1	−2.081	−3.716	−6.725	−6.932	−0.124	−6.326	−6.566	−4.056
CC wave	New scheme 2	−2.087	−3.693	−6.773	−6.974	−0.111	−6.376	−6.711	−4.002

Table 4. Peak value of minimum principal stress at monitoring point under E2 earthquake (MPa)

Seismic wave	Support scheme	Arch crown	Right arch shoulder	Right arch waist	Right arch foot	Arch base	Left arch foot	Left arch waist	Left arch shoulder
EL wave	The original	−2.956	−8.970	−5.809	−11.865	−2.026	−11.401	−6.051	−9.560
EL wave	New scheme 1	−2.887	−8.814	−7.009	−12.155	−1.789	−11.568	−6.881	−9.403
EL wave	New scheme 2	−2.891	−8.757	−7.064	−12.225	−1.808	−11.618	−7.052	−9.332
Hanshin wave	The original	−5.277	−20.041	−8.184	−20.435	−5.846	−20.855	−8.081	−20.311
Hanshin wave	New scheme 1	−5.942	−18.793	−8.439	−20.959	−5.656	−21.371	−8.216	−18.615
Hanshin wave	New scheme 2	−5.938	−18.841	−8.439	−21.003	−5.668	−21.407	−8.329	−18.624
CC wave	The original	−3.050	−10.182	−5.737	−11.338	−2.214	−11.988	−6.249	−8.309
CC wave	New scheme 1	−2.936	−9.907	−6.767	−11.527	−2.092	−12.378	−7.146	−8.290
CC wave	New scheme 2	−2.942	−9.847	−6.811	−11.597	−2.108	−12.437	−7.315	−8.221

Table 5. Peak value of maximum principal stress at monitoring point under E1 earthquake (MPa)

Seismic wave	Support scheme	Arch crown	Right arch shoulder	Right arch waist	Right arch foot	Arch base	Left arch foot	Left arch waist	Left arch shoulder
EL wave	The original	0.041	0.253	−0.280	−0.893	0.872	−0.916	−0.278	0.399
EL wave	New scheme 1	0.051	0.090	−0.390	−1.057	0.826	−0.930	−0.364	0.102
EL wave	New scheme 2	0.041	0.050	−0.380	−1.079	0.825	−0.972	−0.363	0.103
Hanshin wave	The original	0.164	1.889	−0.280	0.841	0.873	0.893	−0.279	1.878
Hanshin wave	New scheme 1	0.185	1.607	−0.400	0.690	0.817	0.903	−0.373	1.562
Hanshin wave	New scheme 2	0.176	1.626	−0.390	0.602	0.820	0.888	−0.371	1.612
CC wave	The original	0.054	0.537	-0.278	−0.906	0.860	−0.914	−0.278	0.320
CC wave	New scheme 1	0.066	0.272	−0.388	−1.064	0.813	−0.957	−0.368	0.078
CC wave	New scheme 2	0.056	0.255	−0.378	−1.086	0.812	-0.997	−0.366	0.080

Table 6. Peak value of minimum principal stress at monitoring point under E2 earthquake (MPa)

Seismic wave	Support scheme	Arch crown	Right arch shoulder	Right arch waist	Right arch foot	Arch base	Left arch foot	Left arch waist	Left arch shoulder
EL wave	The original	0.283	2.164	−0.282	1.508	0.853	1.483	−0.305	2.173
EL wave	New scheme 1	0.323	1.994	−0.389	1.257	0.798	1.315	−0.376	1.959
EL wave	New scheme 2	0.312	2.015	−0.378	1.189	0.802	1.314	−0.374	1.994
Hanshin wave	The original	0.751	2.482	−0.476	1.636	0.891	1.905	−0.471	2.486
Hanshin wave	New scheme 1	0.564	2.465	−0.515	1.368	0.838	1.546	−0.441	2.444
Hanshin wave	New scheme 2	0.541	2.458	−0.504	1.339	0.841	1.567	−0.449	2.437
CC wave	The original	0.336	2.276	−0.281	1.464	0.852	1.601	−0.323	2.145
CC wave	New scheme 1	0.380	2.140	−0.384	1.229	0.797	1.379	−0.378	1.940
CC wave	New scheme 2	0.363	2.151	−0.374	1.157	0.801	1.379	−0.376	1.979

5.3 Plastic Zone Analysis of Tunnel Second Lining Structure

Under E1 seismic action (El-Centro wave, Hanshin wave and CC wave), the post-earthquake plastic zone distribution of tunnel second lining structure of three support schemes is shown in Fig. 3 and Fig. 4.

Under the action of El-Centro wave or Hanshin wave, the post-earthquake plastic zone distribution of the second lining structure of each support scheme is the same, as shown in Fig. 3(a) and Fig. 3(b) respectively.

Figure 3 and Fig. 4 show that the tensile failure area of the tunnel second lining structure of the three support schemes is at the arch bottom. The tensile failure volume is small, and the volume of plastic zone per linear meter is 1.096 m^3–1.436 m^3. Therefore, the tunnel is in a safe and stable state as a whole.

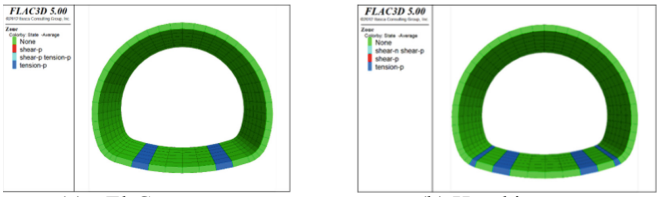

(a) El-Centro wave (b) Hanshin wave

Fig. 3. Plastic zone of tunnel second lining structure during E1 seismic action

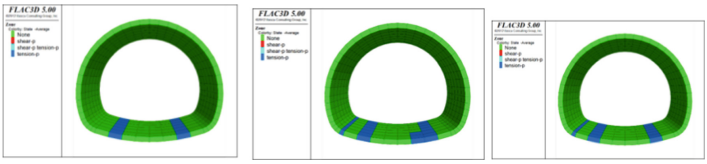

(a) The original (b) New scheme 1 (c) New scheme 2

Fig. 4. Plastic zone of tunnel second lining structure during E1 seismic action (CC wave)

Under E2 seismic action (El-Centro wave, Hanshin wave and CC wave), the post-earthquake plastic zone distribution of tunnel second lining structure of three support schemes is shown in Fig. 5, Fig. 6 and Fig. 7.

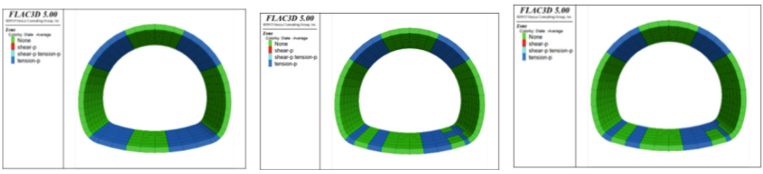

(a)The original (b)New scheme 1 (c)New scheme 2

Fig. 5. Plastic zone of tunnel second lining structure during E2 seismic action (El-Centro wave)

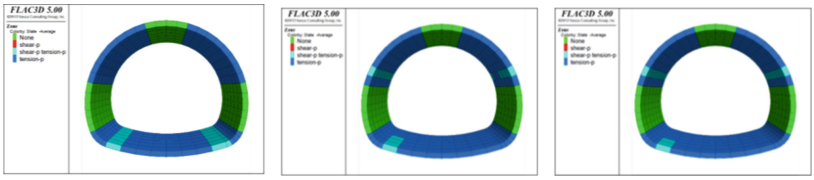

（a）The original （b）New scheme 1 （c）New scheme 2

Fig. 6. Plastic zone of tunnel second lining structure during E2 seismic action (Hanshin wave)

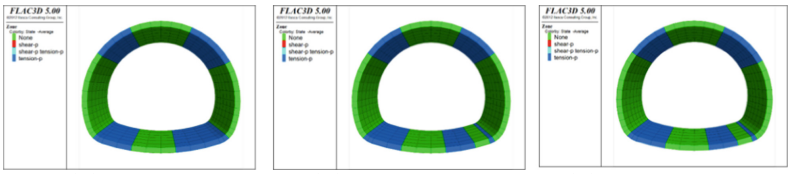

（a）The original （b）New scheme 1 （c）New scheme 2

Fig. 7. Plastic zone of tunnel second lining structure during E2 seismic action (CC wave)

Figure 5, Fig. 6 and Fig. 7 show that under the action of El-Centro wave and CC wave, the failure area of tunnel second lining structure of the three support schemes is conjugate 45° with the horizontal direction, and the distribution area of plastic zone is

mainly concentrated in the spandrel, arch foot and arch bottom, all of which are mainly tensile failure.

Under the action of Hanshin wave, the second lining structure of the tunnel with three support schemes has tensile failure at the arch shoulder, arch foot and arch bottom. Through analysis, it is considered that the natural vibration period of the tunnel structure may be very close to the predominant period of seismic wave, so the seismic response of Hanshin wave is amplified. At the same time, the tunnel second lining structure of the three support schemes produces a small range of shear failure, but the difference of shear failure volume is small. In the original scheme, new New scheme 1 and new scheme 2, the volume of shear failure per linear meter of tunnel second lining structure is 1.266 m^3, 0.780 m^3 and 0.820 m^3 respectively.

Under E2 seismic action (El Centro wave, Hanshin wave and CC wave), the tensile damage volume statistics per linear metre in the plastic zone for the three support schemes after the earthquake are shown in Fig. 8.

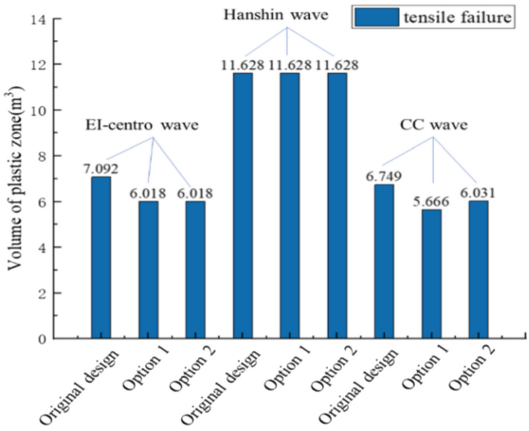

Fig. 8. Volume statistics of the plastic zone of the tunnel second lining structure

As shown in Fig. 8, the amount of tensile damage of the tunnel second lining structure is the same for the three support schemes when Hanshin wave is acting. However, the volume of tensile damage in the plastic zone of the tunnel second lining structure for the new New scheme 1 and 2 is reduced during the action of other seismic waves. The maximum reduction in the tensile damage volume of the tunnel second lining structure for the new New scheme 1 is 16.04% compared to the original scenario for the CC wave action, and the maximum reduction in the tensile damage volume of the tunnel second lining structure for the new scheme 2 is 15.14% compared to the original scenario for the El-Centro wave action. Overall the tensile damage areas produced by the three scenarios are not very different.

Comparing the deformation, stress and plastic zone distribution of the second lining of the three support schemes, it can be seen that the seismic performance of all three is basically the same. Comparing the support measures, it can be seen that the new support

structure reduces the number of anchors used compared to the original support structure. This reduces disturbance to the surrounding rock and has obvious advantages in terms of optimising construction costs, making the new support structure worth promoting.

6 Conclusions

Through the numerical simulation of Xinglinpu tunnel of Yanchong expressway by FLAC3D, this paper analyzed the seismic dynamic response of the tunnel under grade V surrounding rock when the original support structure scheme and the new support structure scheme 1 and 2 were adopted respectively. The following conclusions are drawn:

(1) Under E1 seismic action, the compressive stress of tunnel second lining structure in the three support schemes is less than the standard value of dynamic compressive strength of C35 concrete, and the tensile stress is less than the standard value of dynamic tensile strength of C35 concrete. There is less plastic damage at the bottom of the plastic zone of the second lining structure after the earthquake. The tunnel structure meets the requirements of "no damage in small earthquake" and is safe and stable as a whole.
(2) Under E2 seismic action, the maximum convergence value of tunnel second lining structure in the three support schemes is less than the maximum convergence value (5‰ of tunnel span) required in the code. The plastic failure area of the second lining structure after the earthquake is conjugate 45° with the horizontal direction, which is mainly concentrated at the arch shoulder and arch foot. The plastic zone of the whole second lining structure is not penetrated, which is local failure and meets the “repairable level under moderate earthquake action”.
(3) Compared with the seismic performance of the original support structure scheme and the new support structure scheme, the seismic performance of the two schemes is basically the same. The new support structure reduces the number of anchors, so it can reduce the disturbance to the surrounding rock. Because of its obvious advantages in construction cost optimization, the new support structure is worth popularizing.

Acknowledgement. This paper is obtained, based on the research project “Research Projects of the Hebei Provincial Department of Transport (YC-201906)”.

References

1. Jian, M.A., et al.: Review on China’s tunnel engineering research. China J. Highway Transp. **5**, 1–65 (2015)
2. Qian, Q.H., He, C., Yan, Q.X.: Investigation and study of seismic damage of Wenchuan earthquake. Chin. Soc. Rock Mech. Eng., 633–643 (2009)

3. Sun, Q.Q., Dias, D.: Seismic behavior of circular tunnels Influence of the initial stress state. Soil Dyn. Earthq. Eng. **126**, 1–17 (2019)
4. Yan, L.Q., Haider, A., Li, P., et al.: A numerical study on the transverse seismic response of lined circular tunnels under obliquely incident asynchronous P and SV waves. Tunn. Undergr. Space Technol. **97**, 103232 (2020)
5. Wang, M.N., Cui, G.Y.: Establishment of tunnel damping model and research on damping effect with model test in highly seismic area. Rock Soil Mech. **06**, 1884–1890 (2010)
6. Cui, G.Y., Wang, L.B., Wang, M.N., et al.: Model experimental study of rigid-flexible seismic mitigation measures in soft rock cavern sections of tunnels in strong earthquake zones. J. Vibr. Eng. **01**, 29–36 (2019)
7. Jiang, S.P., Wen, D.L., Zhang, S.B.: Large-scale shaking table test for seismic response in portal section of galongla tunnel. Chin. J. Rock Mech. Eng. **04**, 649–656 (2011)
8. Wang, Q.Y., Yang, K., Mao, J.L., et al.: Research on comprehensive seismic measures for secondary lining structures of highway tunnels in nine-degree seismic zones. Mod. Tunn. Technol. **05**, 42–49 (2019)
9. Liang, B., Zhao, F.B., Ren, Z.D., et al.: Analysis on seismic response of a super-large section tunnel in highway. Chin. J. Undergr. Space Eng. **01**, 243–248 (2020)
10. He, Z.G., Wang, X.W., Zuo, Z.B.: Numerical analysis of seismic response of lining structure for portal section in mountain tunnel. Sci. Technol. Eng. **17**, 7018–7024 (2020)
11. Liu, L.Y., Chen, Z.Y., Yuan, Y.: Impact of rock class on seismic responses of mountain tunnels under severe earthquakes. Chin. J. Undergr. Space Eng. **S1**, 1314–1318 (2011)
12. Xu, D.Q., Li, Y.Q., Zhang, N., et al:. Integrated support structure and construction process of highway tunnel primary lining steel arch with prestressed anchor CN206220978U (2017)
13. China Earthquake Administration, Seismic ground motion parameters zonation map of China (GB 18306–2015) Standards Press of China (2015)
14. Chongqing Communication Technology Research and Design Institute, Specifications for design of highway tunnels (JTG 3370.1–2018) China Communications Press (2018)
15. Zhang, L.Y., Zhang, Q.Y., Li, S.C., et al.: Analysis of impact of surrounding rock post-grouting for large oil cavern on its water seal ability based on fluid-solid coupling. Rock Soil Mech. **S2**, 474–480 (2014)
16. Chongqing Communication Technology Research and Design Institute, Specifications for Seismic Design of Highway Tunnels (JTG 2232–2019) China Communications Press (2019)